2022

m6A modifications regulate intestinal immunity and rotavirus infection

Anmin Wang

Gaopeng Hou

Siyuan Ding

et al

RESEARCH ARTICLE

m6A modifications regulate intestinal immunity and rotavirus infection

Anmin Wang[1,2], Wanyiin Tao[1,2], Jiyu Tong[3], Juanzi Gao[1], Jinghao Wang[1], Gaopeng Hou[4], Chen Qian[1], Guorong Zhang[1,2], Runzhi Li[1,2], Decai Wang[1,2], Xingxing Ren[1,2], Kaiguang Zhang[1], Siyuan Ding[4], Richard A Flavell[5,6], Huabing Li[3], Wen Pan[1,2]*, Shu Zhu[1,2,7,8]*

[1]Department of Digestive Disease, The First Affiliated Hospital of University of Science and Technology of China, Division of Life Sciences and Medicine, University of Science and Technology of China, Hefei, China; [2]Institute of Immunology, the Chinese Academy of Sciences Key Laboratory of Innate Immunity and Chronic Disease, Division of Life Sciences and Medicine, University of Science and Technology of China, Hefei, China; [3]Shanghai Institute of Immunology, Department of Microbiology and Immunology, Shanghai Jiao Tong University School of Medicine (SJTU-SM), Shanghai, China; [4]Department of Molecular Microbiology, Washington University School of Medicine in St. Louis, St. Louis, United States; [5]Department of Immunobiology, Yale University School of Medicine, New Haven, United States; [6]Howard Hughes Medical Institute, Yale University School of Medicine, New Haven, United States; [7]School of Data Science, University of Science and Technology of China, Hefei, China; [8]Institute of Health and Medicine, Hefei Comprehensive National Science Center, Hefei, China, Hefei, China

Abstract N6-methyladenosine (m6A) is an abundant mRNA modification and affects many biological processes. However, how m6A levels are regulated during physiological or pathological processes such as virus infections, and the in vivo function of m6A in the intestinal immune defense against virus infections are largely unknown. Here, we uncover a novel antiviral function of m6A modification during rotavirus (RV) infection in small bowel intestinal epithelial cells (IECs). We found that rotavirus infection induced global m6A modifications on mRNA transcripts by down-regulating the m6a eraser ALKBH5. Mice lacking the m6A writer enzymes METTL3 in IECs (*Mettl3*ΔIEC) were resistant to RV infection and showed increased expression of interferons (IFNs) and IFN-stimulated genes (ISGs). Using RNA-sequencing and m6A RNA immuno-precipitation (RIP)-sequencing, we identified IRF7, a master regulator of IFN responses, as one of the primary m6A targets during virus infection. In the absence of METTL3, IECs showed increased *Irf7* mRNA stability and enhanced type I and III IFN expression. Deficiency in IRF7 attenuated the elevated expression of IFNs and ISGs and restored susceptibility to RV infection in *Mettl3*ΔIEC mice. Moreover, the global m6A modification on mRNA transcripts declined with age in mice, with a significant drop from 2 weeks to 3 weeks post birth, which likely has broad implications for the development of intestinal immune system against enteric viruses early in life. Collectively, we demonstrated a novel host m6A-IRF7-IFN antiviral signaling cascade that restricts rotavirus infection in vivo.

Editor's evaluation

This study clearly shows that m6A modification on mRNA regulates immune responses in the intestine during rotavirus infection. The authors further show the mechanisms how m6A modification is

***For correspondence:** wenpan@ustc.edu.cn (WP); zhushu@ustc.edu.cn (SZ)

Competing interest: The authors declare that no competing interests exist.

Funding: See page 16

Received: 06 September 2021
Preprinted: 17 September 2021
Accepted: 28 January 2022
Published: 31 January 2022

Reviewing Editor: Kiyoshi Takeda, Osaka University, Japan

regulated in the intestine. Thus, this study provides important insights into the regulation of anti-viral immunity in the intestine.

Introduction

N6-methyladenosine (m6A) is the most abundant internal mRNA modification and modulates diverse cellular functions through m6A-related writers, erasers, and readers (**Roundtree et al., 2017**; **Xu et al., 2021**; **Chelmicki et al., 2021**). The m6A modification directly recruits m6A-specific proteins of the YT521-B homology (YTH) domain family (**Roundtree et al., 2017**). These proteins mediate the m6A-dependent regulation of pre-mRNA processing, microRNA processing, translation initiation, and mRNA decay (**Roundtree et al., 2017**). In recent works, m6A modifications has been identified in the genomes of RNA viruses and the transcripts of DNA viruses with either a pro-viral or anti-viral role (**Tsai et al., 2018**; **Li et al., 2017**; **Hesser et al., 2018**; **Imam et al., 2018**; **Ye et al., 2017**). Furthermore, m6A RNA modification-mediated down-regulation of the α-ketoglutarate dehydrogenase (KGDH)-itaconate pathway inhibits viral replication independent of the innate immune response (**Liu, 2019**). According to **Gao et al., 2020**, m6A modification preserves the self-recognition of endogenous transcripts. Deletion of the m6A writer *Mettl3* decreases the m6A modifications in endogenous retrovirus (ERV) transcripts. The accumulation of ERVs activates pattern recognition receptors (e.g. RIG-I) pathways, resulting in a detrimental interferon response in livers of fetal mice (**Gao et al., 2020**).

The m6A modification of the enterovirus 71 (EV71) RNA genome is important for viral propagation, and EV71 infection increases the expression of m6A writers in vitro (**Hao et al., 2019**). m6A methyltransferase METTL3 knockdown reduces whereas m6A demethylase FTO knockdown increases EV71 replication (**Hao et al., 2019**). In addition, human cytomegalovirus can upregulate the expression of m6A-related proteins (**Rubio et al., 2018**; **Winkler et al., 2019**). Despite the knowledges about m6A regulation and function during viral infection revealed by these in vitro studies, the regulation of m6A modifications and the specific role of m6A in the antiviral response in vivo, especially in the gastrointestinal tract, remains unclear.

Rotavirus (RV), a member of the family *Reoviridae*, is a nonenveloped icosahedral-structured virus with 11 segments of double-stranded RNA. Children under the age of five are at high risk of rotavirus infection, which causes severe diarrhea, dehydration, and death (**Crawford et al., 2017**). Rotaviruses encode multiple viral proteins to inhibit innate immune responses by degrading interferon regulatory factors (IRFs) and mitochondrial antiviral-signaling protein (MAVS), thus facilitating efficient virus infection and replication (**Ding et al., 2018**; **Barro and Patton, 2007**). The timely induction of an IFN response is key to the host successful control of invading viruses, including RV (**Honda et al., 2005**; **Lin et al., 2016**; **Pott et al., 2011**). Here, we found rotavirus infection induced global m6A modifications on mRNA transcripts by down-regulating the m6A eraser ALKBH5. Mice lacking the m6A writer enzymes METTL3 in IECs (*Mettl3*ΔIEC) were resistant to RV infection. We identified IRF7, a master regulator of IFN responses (**Honda et al., 2005**), as one of the primary m6A targets during virus infection. In the absence of METTL3, IECs showed increased *Irf7* mRNA stability and enhanced type I and III IFN expression. Deficiency in IRF7 attenuated the elevated expression of IFNs and ISGs and restored susceptibility to RV infection in *Mettl3*ΔIEC mice. Collectively, we identified a novel regulation and function of m6A modifications in an enteric viral infection model in vivo.

Results

The regulation and function of mRNA m6A modifications during RV infection

RV infections primarily take place in children under the age of five in humans and in neonatal mice younger than 2 weeks old (**Crawford et al., 2017**; **Du et al., 2017**). Intriguingly, total RNA m6A modifications in the mouse ileal tissues, revealed by a m6A dot blot and mass spectrum (MS) analysis, significantly declined from 2 weeks to 3 weeks post birth (**Figure 1a, b and c**), which caused by increased *Alkbh5* expression (**Figure 1d**, **Figure 1—figure supplement 1a** and **Figure 1—figure supplement 1b**) and development of microbiota might be involved (**Figure 1—figure supplement 2**). Indeed, overexpression of *Alkbh5* in mouse IEC cell line caused decreased m6A level (**Figure 1—figure**

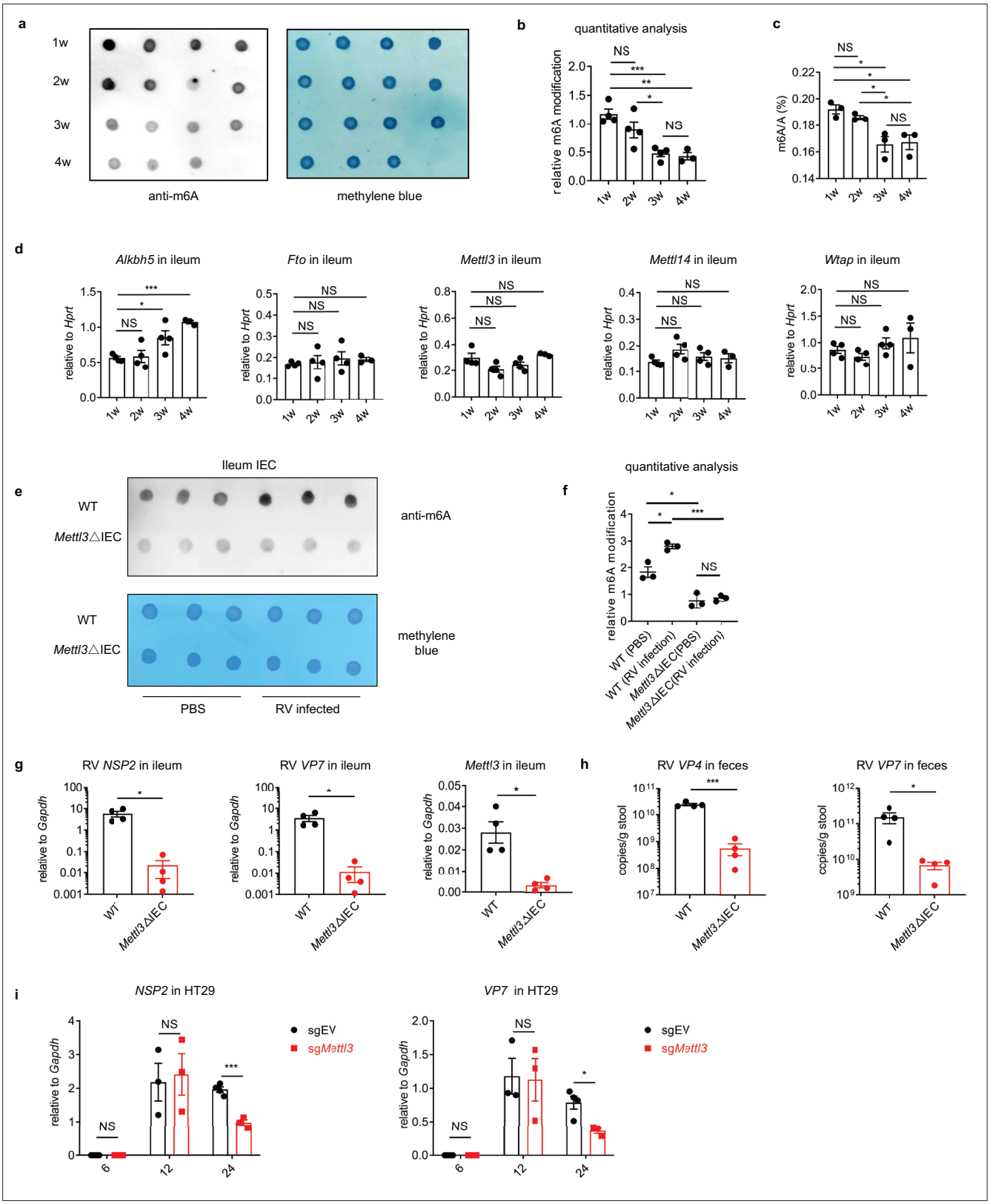

Figure 1. Rotavirus infection increases global m6A modifications, and METTL3 deficiency in IECs results in increased resistance to rotavirus infection. (**a**) m6A dot blot analysis of total RNA in ileum tissues from mice with different ages. Methylene blue (MB) staining was the loading control. (**b**) Quantitative analysis of (**a**) (mean ± SEM), statistical significance was determined by Student's t-test (**p < 0.005, ***p < 0.001, NS., not significant). The quantitative m6A signals were normalized to quantitative MB staining signals. (**c**) mass spectrum (MS) analysis of m6A level in ileum tissue from

Figure 1 continued on next page

Figure 1 continued

mice with different ages. (mean ± SEM), Statistical significance was determined by Student's t-test (*p < 0.05, NS., not significant). (**d**) qPCR analysis of indicated genes in ileum tissues from mice with different ages (mean ± SEM). Statistical significance was determined by Student's t-tests between groups (*p < 0.05, ***p < 0.001, NS., not significant). (**e**) WT and *Mettl3*ΔIEC mice were infected by rotavirus EW strain at 8 days post birth. m6A dot blot analysis of total RNA in ileum IEC at 2 dpi. Methylene blue (MB) staining was the loading control. (**f**) Quantitative analysis of (**e**) (mean ± SEM). Statistical significance was determined by Student's t-test (*p < 0.05, ***p < 0.001, NS., not significant). The quantitative m6A signals were normalized to quantitative MB staining signals. (**g–h**) *Mettl3*ΔIEC mice and littermate controls were infected by rotavirus EW strain at 8 days post birth. qPCR analysis of RV viral loads in ileum tissue (**g**) or fecal samples (**h**) from *Mettl3*ΔIEC mice and littermate controls at 4 days post infection (dpi) (littermate WT n = 4, *Mettl3*ΔIEC n = 4, mean ± SEM). Statistical significance was determined by Student's t-tests between genotypes (*p < 0.05). (**i**) qPCR analysis of indicated genes in Rhesus rotavirus (RRV)-infected HT-29 cells transduced with *Mettl3* sgRNA or control sgRNA, at indicated hours post infection (hpi) (mean ± SEM), statistical significance was determined by Student's t-test (*p < 0.05, ***p < 0.001, NS., not significant). Experiments in (**a, d-f, and i**) are repeated twice, (**g and h**) are repeated four times.

The online version of this article includes the following figure supplement(s) for figure 1:

Figure supplement 1. ALKBH5 regulates total RNA m6A modification level in intestine.

Figure supplement 2. Dot blot analysis of total RNA m6A modification level in the ileum of germ-free mice.

Figure supplement 3. Mass spectrum (MS) analysis of total RNA m6A modification level in RV infected ileum.

Figure supplement 4. Schematic design of RV infection model.

supplement 1c), supporting the role of *Alkbh5* in regulating global m6A levels in intestine. These data indicating a potential link between the resistance to RV infection and the decline of m6A modification during early life development.

Besides, the global m6A RNA modification levels increased in the ileum tissue of suckling mice post RV murine strain EW infection (***Figure 1e and f*** and ***Figure 1—figure supplement 3***). As a control, the m6A modification can barely detected in IECs deficiency with m6A writer METTL3 (*Mettl3*$^{fl/fl}$*Vil1*^{Cre}, *Mettl3*ΔIEC) (***Figure 1e and f***). Thus, we hypothesize that RV may induce an enriched cellular m6A modification environment and a weakened innate immune response to facilitate virus replication. To investigate the in vivo role of m6A in the anti-RV immunity, we infected *Mettl3*ΔIEC mice and wild-type (WT) littermates with RV EW strain. The viral RNA load in *Mettl3*ΔIEC mice ileum tissue was significantly lower than that in the WT mice (***Figure 1g*** and ***Figure 1—figure supplement 4***). Fecal virus shedding was also significantly lower in *Mettl3*ΔIEC mice (***Figure 1h***). Genetic knockdown of METTL3 in HT-29 cells, a human colonic epithelial cell line, by CRISPR-mediated gene silencing, also led to reduced RV replication (***Figure 1i***), further highlighting the resistance phenotype to RV infection by METTL3 deficiency.

METTL3 deficiency in IECs results in decreased m6A deposition on *Irf7*, and increased interferon responses

To dissect the underlying mechanism, we performed RNA-sequencing using the IECs from METTL3-deficient mice and littermate controls at steady state. Most of the differentially expressed genes in METTL3-deficient IECs vs WT IECs were enriched in the pathways of 'defense response to virus', 'response to interferon-beta', and 'positive regulation of innate immune response' by gene ontology analysis (***Figure 2a***). Heatmap also showed that a panel of interferon stimulate genes (ISGs) are upregulated in METTL3-deficient IECs compared to WT IECs (***Figure 2b***). To map potential m6A modification sites on mRNAs of these differential expressed genes in IECs, we conducted m6A RIP-sequencing based on a previously reported protocol (***Li et al., 2017***). Metagene plots showed the m6A peak is enriched near the stop codon and 3'-UTR region, which is consistent with previously studies (***Xuan et al., 2018***; ***Dominissini et al., 2012***; ***Figure 2—figure supplement 1b***). We found that m6A modified one of the master regulators of IFNs, *Irf7* (***Figure 2c***), which played a key role in the network of these differential expressed genes in METTL3-deficient IECs compared to WT IECs, analyzed by STRING (***Figure 2d***). Of note, *Irf7* was the only IRFs that highly expressed in METTL3-deficient IECs, and *Irf7* was the prominently highest expressed *Irf* in IECs (***Figure 2e***), indicating *Irf7* might be one of the key genes that are modulated by m6A modifications. We also validated our results by m6A RIP-qPCR to examine m6A modification sites in *Irf7* mRNA based on our RIP-sequencing data in METTL3 knock-down MODE-K cells and predicted results from the database (http://rna.sysy.edu.cn) (***Figure 2—figure supplement 1a***, ***Figure 2—figure supplement 1c*** and ***Figure 2—figure supplement 1d***). It should be noted that our m6A-RIP-seq were performed at steady state. We did not

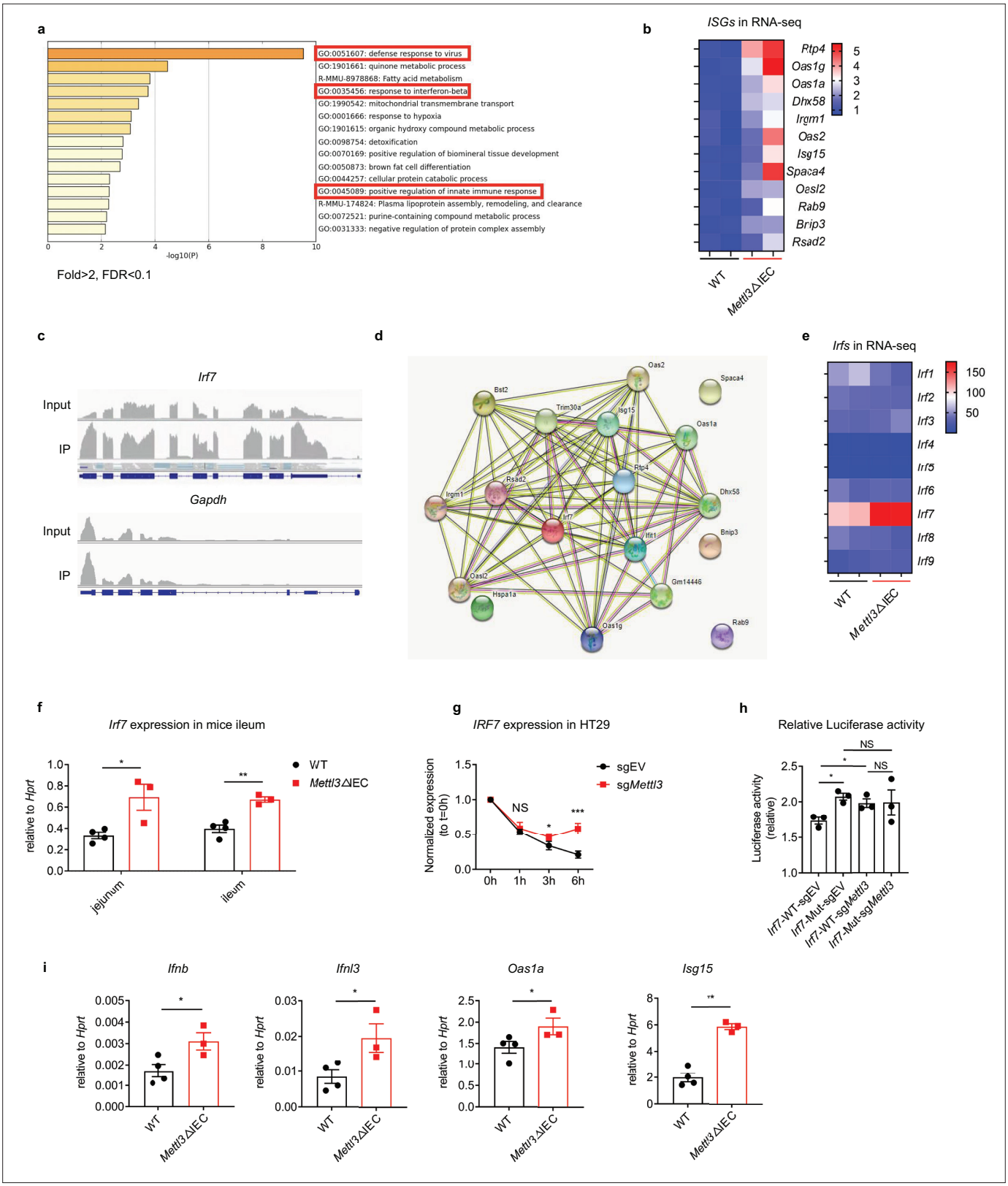

Figure 2. METTL3 deficiency in IECs results in decreased m6A deposition on *Irf7*, and increased interferon responses. (**a**) Gene ontology (GO) analysis of differentially expressed genes in IECs from *Mettl3*ΔIEC mice vs IECs from littermate WT mice. (**b**) Heat map of a subset of upregulated *ISGs* in IECs from *Mettl3*ΔIEC mice vs IECs from littermate WT mice, as revealed by RNA-seq (normalized data). (**c**) m6A-RIP-seq analysis of *Irf7* and *Gapdh* mRNA in the ileum of WT mice. (**d**) Gene regulation network of a subset of up-regulated genes including IRF7. (**e**) Heat map of Interferon regulatory factors

Figure 2 continued on next page

Figure 2 continued

(*Irfs*) in IECs from *Mettl3*ΔIEC mice vs IECs from littermate WT mice, as revealed by RNA-seq (RPKM). (**f**) *Mettl3*ΔIEC mice and littermate controls were infected by EW at 8 days post birth. qPCR analysis of the *Irf7* expression in ileum and jejunum from *Mettl3*ΔIEC mice and littermate control at 2 dpi (littermate WT n = 4, *Mettl3*ΔIEC mice n = 3, mean ± SEM). Statistical significance was determined by Student's t-test (*p < 0.05, **p < 0.005). (**g**) q-PCR analysis of *Irf7* mRNA in METTL3 knockdown HT-29 cells or control cells in indicated time points post actinomycin D treatment (n = 3, mean ± SEM). Statistical significance was determined by Student's t-test (*p < 0.05, ***p < 0.001, NS., not significant). (**h**) Relative luciferase activity of sgEV and sg*Mettl3* HEK293T cells transfected with pmirGLO-*Irf7*-3'UTR (*Irf7*-WT) or pmirGLO-*Irf7*-3'UTR containing mutated m6A modification sites (*Irf7*-MUT). The firefly luciferase activity was normalized to Renilla luciferase activity (n = 3, mean ± SEM). Statistical significance was determined by Student's t-tests between groups (*p < 0.05, NS., not significant). (**i**) *Mettl3*ΔIEC mice and littermate control and were infected by EW at 8 days post birth. qPCR analysis of selected *IFNs* and *ISGs* in ileum tissue at two dpi (littermate WT, n = 4, *Mettl3*ΔIEC mice, n = 3, mean ± SEM). Statistical significance was determined by Student's t-tests between genotypes (*p < 0.05, **p < 0.005). Experiments in (**f, h and i**) are repeated three times, (**g**) are repeated twice.

The online version of this article includes the following figure supplement(s) for figure 2:

Figure supplement 1. Characterization of m6A modifications on *Irf7* mRNA.

Figure supplement 2. METTL3 knockdown in HT-29 cells results in increased IFN response.

Figure supplement 3. METTL3 deficiency in MA104 cells results in increased resistance to Rhesus rotavirus infection.

Figure supplement 4. m6A modification on Irf7 mRNA regulates its expression.

Figure supplement 5. Expression of *Irf7* and *ISGs* in ileum from mice during early life development.

identified previous reported *Ifns* (***Rubio et al., 2018***; ***Winkler et al., 2019***), possibly due to the low expression level of *Ifns* in IECs at steady state.

IRF7 is a known master regulator of Type I interferon and Type III interferon-dependent immune responses in respond to virus infection (***Barro and Patton, 2007***; ***Honda et al., 2005***; ***Ciancanelli et al., 2016***). We reasoned that loss of m6A modification on *Irf7* mRNA is responsible for the increased IFN response and subsequent resistance to RV infection. Thus, we first validated the regulation of *Irf7* mRNA levels by m6A in mice and in cells. We found an increase of *Irf7* mRNA in ileum tissue of *Mettl3*ΔIEC mice compared to that in WT littermate control mice (***Figure 2f***). Consistently, the expression of *IRF7* mRNA was also higher in METTL3 knockdown HT-29 and *METTL3* knockout rhesus monkey MA104 cells, suggesting that the regulation of *IRF7*/*Irf7* expression by m6A is likely conserved across species (***Figure 2—figure supplement 2***, ***Figure 2—figure supplement 3***). Furthermore, genetic knockdown of METTL3 in human or mice IEC cell lines also led to increased *IRF7*/*Irf7* expression and *IFN*/*Ifn* responses (***Figure 2—figure supplement 1f***, ***Figure 2—figure supplement 2***). As m6A is known to regulate the mRNA decay, we next sought to determine whether the stability of *IRF7* mRNA is regulated by m6A. We used actinomycin D to block the de novo RNA synthesis in HT-29 cells to assess the RNA degradation by METTL3 knockdown. The *IRF7* mRNA degraded significantly slower in METTL3-knockdown HT-29 cells than the control cell line (***Figure 2g***, ***Figure 2—figure supplement 2b***).

To directly evaluate the role of m6A in modulating the stability of *Irf7* mRNA, luciferase reporter assays were conducted. In comparison with wild-type *Irf7*-3'UTR (*Irf7*-WT) constructs, the ectopically expressed constructs harboring m6A mutant *Irf7*-3'UTR (*Irf7*-MUT) showed significantly increased luciferase activity (***Figure 2h***, ***Figure 2—figure supplement 1e***). Further, mutation of m6A modification sites can directly increase the expression of *Irf7* and enhance the antiviral function of *Irf7* in MEF cells (***Figure 2—figure supplement 4a*** and ***Figure 2—figure supplement 4b***). These results suggest that the upregulation of *Irf7* mRNA level in *Mettl3*ΔIEC mice is caused by the loss of m6A modification mediated mRNA decay. To evaluate the potential influence of m6A on *Irf7* transcriptional targets, we also measured the expressions of IFNs and ISGs in rotavirus infected ileum tissue from *Mettl3*ΔIEC mice and littermate WT mice. We found the transcriptional targets of *Irf7*, were all upregulated in *Mettl3*ΔIEC mice (***Figure 2i***). Furthermore, we found that the mRNAs of *Irf7* and its transcriptional targets ISGs increased in the ileum of the mice from 1 to 4 weeks, with a dramatic upregulation from 2 to 3 weeks (***Figure 2—figure supplement 5***), which was concomitant with the decrease of global m6A modifications (***Figure 1a and b*** and ***Figure 1—figure supplement 1a***). These results demonstrated that METTL3 deficiency in IECs results in decreased m6A deposition on *Irf7*, and increased interferon response.

IRF7 deficiency attenuated the increased interferon response and resistance to RV infection in *Mettl3*ΔIEC mice

To determine whether *Irf7* plays a key role in the resistance phenotype to RV infection in METTL3-deficient mice in IECs, we crossed *Irf7*$^{-/-}$ mice to *Mettl3*ΔIEC mice. Following RV oral gavage, the

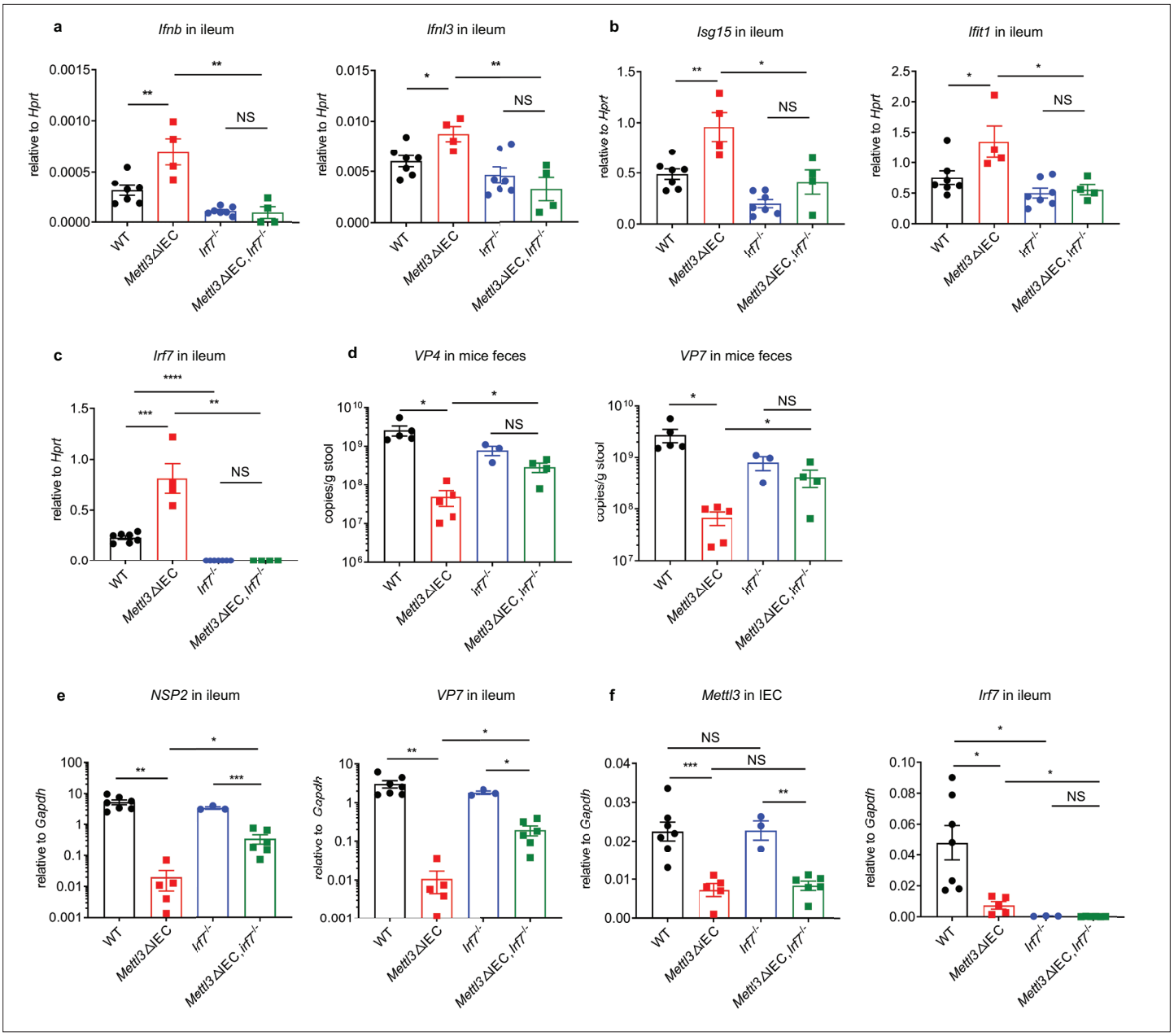

Figure 3. IRF7 deficiency attenuated the increased interferon response and resistance to rotavirus infection in *Mettl3*ΔIEC mice. (**a–c**) WT control mice, *Mettl3*ΔIEC mice, *Irf7*$^{-/-}$ mice and *Mettl3*ΔIEC *Irf7*$^{-/-}$ mice are all littermates. They were infected by RV EW at 8 days post birth. qPCR analysis of selected *IFNs* (**a**), *ISGs* (**b**), or *Irf7* (**c**) expression in ileum from indicated groups of mice at two dpi (littermate WT n = 7, *Mettl3*ΔIEC n = 5, *Irf7*$^{-/-}$ n = 3, *Mettl3*ΔIEC *Irf7*$^{-/-}$ n = 6, mean ± SEM). Statistical significance was determined by Student's t-tests between genotypes (*p < 0.05, **p < 0.005, ***p < 0.001, ****p < 0.0001, NS., not significant). (**d**) qPCR analysis of fecal rotaviral shedding in indicated groups of mice at four dpi (littermate WT n = 5, *Mettl3*ΔIEC n = 5, *Irf7*$^{-/-}$ n = 3, *Mettl3*ΔIEC *Irf7*$^{-/-}$ n = 4, mean ± SEM). Statistical significance was determined by Student's t-tests between genotypes (*p < 0.05, **p < 0.005, NS., not significant). (**e–f**) qPCR analysis of RV proteins expression (**e**) or *Mettl3* and *Irf7* (**f**) in ileum from indicated groups of mice at four dpi (littermate WT n = 7, *Mettl3*ΔIEC n = 5, *Irf7*$^{-/-}$ n = 3, *Mettl3*ΔIEC *Irf7*$^{-/-}$ n = 6, mean ± SEM). Statistical significance was determined by Student's t-tests between genotypes and (*p < 0.05, **p < 0.005, ***p < 0.001, NS., not significant). Experiments in (**a–f**) are repeated twice.

expression of IFNs and ISGs in ileum from *Irf7*$^{-/-}$*Mettl3*ΔIEC mice were significantly lower than those from *Mettl3*ΔIEC mice at 2dpi (***Figure 3a–c***), and unlike the increased expression of IFNs and ISGs in *Mettl3*ΔIEC mice vs littermate WT controls, by deficiency of IRF7, the expression of IFNs and ISGs in ileum from *Irf7*$^{-/-}$*Mettl3*ΔIEC mice were not significantly different from those from *Irf7*$^{-/-}$ mice

(***Figure 3a–c***), suggesting that *Irf7* mediates the increased expression of IFNs and ISGs in *Mettl3*ΔIEC mice.

Moreover, the *Irf7*$^{-/-}$*Mettl3*ΔIEC mice showed significantly higher viral loads in ileum tissue and higher fecal shedding of RV *Mettl3*ΔIEC (***Figure 3d–f***). Similarly, unlike the much lower fecal viral shedding in *Mettl3*ΔIEC mice vs littermate WT controls, by deficiency of IRF7, the fecal viral shedding in *Irf7*$^{-/-}$*Mettl3*ΔIEC mice were not significantly different from those in *Irf7*$^{-/-}$ mice (***Figure 3d***), suggesting that *Irf7* mediates the resistant phenotype of rotavirus infection measured by fecal viral shedding in *Mettl3*ΔIEC mice. Notably, the viral proteins expression difference in ileum from *Irf7*$^{-/-}$*Mettl3*ΔIEC mice vs that from *Irf7*$^{-/-}$ mice (9.7-fold lower for NSP2 and 9.3-fold lower for VP7), was much lower than the viral proteins expression difference in ileum from *Mettl3*ΔIEC mice vs that from littermate mice (267.1-fold lower for NSP2 and 283.4-fold lower for VP7) (***Figure 3e***), suggesting that besides the contribution of *Irf7* to the resistant phenotype of rotavirus infection in IECs from *Mettl3*ΔIEC mice, other pathways (e.g. m6A modifications in RV RNA) may also play roles. Therefore, IRF7 is an important mediator of the increased IFNs and ISGs expression in *Mettl3*ΔIEC mice and genetic deletion of IRF7 restored the resistant phenotype of *Mettl3*ΔIEC mice to RV infection.

Rotavirus suppresses ALKBH5 expression through NSP1 to evade immune defense

We next sought to determine how RV regulates the m6A modifications in IECs. We first measured whether RV infection regulates the m6A-related writer and eraser proteins in the intestine. The protein levels of the methyltransferases METTL3 and METTL14 and demethylase FTO were not affected by RV infection in ileum tissue (***Figure 4a and b***). In contrast, the protein level of demethylase ALKBH5 was significantly down-regulated by RV infection in the ileum (***Figure 4a and b***). To determine whether ALKBH5 play a role in anti-RV infection since it's suppressed during RV infection, we generated the IEC-specific deletion of ALKBH5 in mice (*Alkbh5*$^{fl/fl}$ *Vil1*^{Cre}, *Alkbh5*ΔIEC). The depletion of ALKBH5 in IECs did not affected the anti-RV immune response (***Figure 4c***), the viral shedding in the feces (***Figure 4d***), or the viral protein expression in the ileum (***Figure 4e***), likely due to the suppressed ALKBH5 expression in ileum tissue of WT mice infected by RV.

We next asked whether there is redundancy between m6A eraser ALKBH5 and FTO. We first checked the expression of *Alkbh5/ALKBH5* and *Fto/FTO* in our RNA-seq data in mouse IECs, and also a previous reported RNA-seq data in human intestinal enteroid (***Saxena et al., 2017***). We found the *Alkbh5/ALKBH5* expression is much higher than *Fto/FTO* in intestine (***Figure 4—figure supplement 1a***). We did qPCR analysis in mouse epithelial cell line MODE-K and showed the similar results (***Figure 4—figure supplement 1a***). Furthermore, we knock down METTL3, ALKBH5 and FTO in MODE-K cell. Through dot blot assay, we found ALKBH5 but not FTO is the dominant m6A eraser in IECs (***Figure 4—figure supplement 1***). Furthermore, overexpressing of recombinant ALKBH5 increased the IFN/ISGs response and inhibit RRV infection in mouse IEC MODE-K cells (***Figure 4—figure supplement 2***), suggesting re-expression of ALKBH5 might overcome the immune evasion of RV.

Non-structural protein 1 (NSP1) is a well-established RV-encoded innate immune antagonist that are showed to degrade IRF3 and β-Trcp (***Barro and Patton, 2005***; ***Ding et al., 2016***). To test the potential role of NSP1 in AlKBH5 inhibition, we used the recently developed reverse genetics system and rescued recombinant WT RV SA11 strain and a mutant virus that does not express NSP1 (NSP1-null) (***Kanai et al., 2017***). We infected HEK293 cells with WT and NSP1-null RVs, only WT RV reduced ALKBH5 protein levels (***Figure 4f***), suggesting that the down-regulation of ALKBH5 expression by RV is NSP1-dependent. These results suggest that RV might evades the antiviral immune response via downregulation of ALKBH5 expression by NSP1.

Discussion

Previous studies reported that m6A modifications on mRNA in mice embryonic fibroblasts or normal human dermal fibroblasts negatively regulate the IFN response by accelerating the mRNA degradation of type I IFNs (***Rubio et al., 2018***; ***Winkler et al., 2019***). However, these studies were mainly conducted in vitro, leaving the relationship between m6A and IFN pathway in vivo an unexplored territory. Since type I and type III IFNs play a critical role in the antiviral immune response in the GI

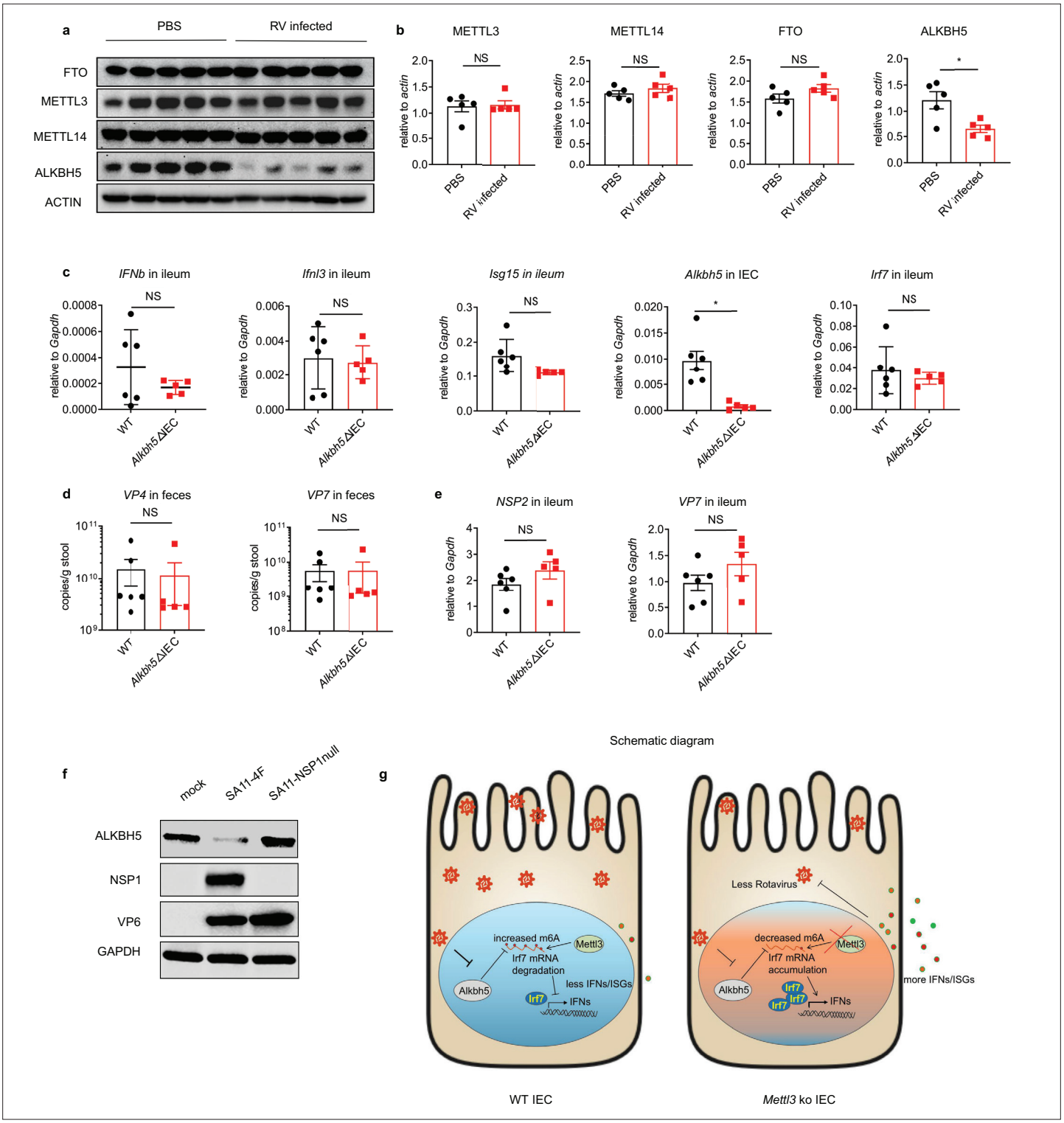

Figure 4. Rotavirus suppresses ALKBH5 expression through NSP1 to evade immune defense. (**a**) WT mice were infected by RV EW at 8 days post birth. Immunoblotting with antibodies target ALKBH5, FTO, METTL14 and METTL3 in ileum tissue from mice infected with RV EW at two dpi or treated with PBS. (**b**) Quantitative analysis of (**a**) (mean ± SEM), Statistical significance was determined by Student's t-test (*p < 0.05). (**c–e**) *Alkbh5*ΔIEC mice and littermate controls were infected by RV EW at 8 days post birth. qPCR analysis of indicated genes expression in ileum (**c**), viral shedding in feces (**d**), and viral proteins expression in ileum (**e**), from *Alkbh5*ΔIEC mice or littermate controls at 4 days post infection (littermate WT n = 6, *Alkbh5*ΔIEC n = 5, mean ± SEM). Statistical significance was determined by Student's t-tests between genotypes (*p < 0.05, NS., not significant). (**f**) Immunoblotting with antibodies target ALKBH5, NSP1, VP6 and GAPDH in HEK293 cells infected by SA11-4F and SA11-NSP1null (MOI = 1) for 24 hr. (**g**) Graphical abstract

Figure 4 continued on next page

Figure 4 continued

illustrating the functions and molecular mechanisms of m6A modifications on *Irf7* in anti-RV infection. Experiments in (**a–e**) are repeated three time, (**f**) are repeated twice.

The online version of this article includes the following figure supplement(s) for figure 4:

Figure supplement 1. A non-redundant role of *Alkbh5* in regulating m6A modification in IECs.

Figure supplement 2. ALKBH5 over-expression in MODE-K cells results in enhanced IFN response and increased resistance to Rhesus rotavirus infection.

Figure supplement 3. m6A-RIP-qPCR analysis of the predicted m6A sites on Rotavirus RNA.

Figure supplement 4. METTL3 deficiency leads to aberrant dsRNA formation in isolated IECs.

tract (***Pott et al., 2011***), we used an RV infection model, in which IECs are specifically infected, as well as conditional knockout mice with IECs-specific depletion of m6A writer METTL3 or m6A eraser ALKBH5, to study the role of m6A modification in regulating IFN response towards rotavirus in IECs. Using RNA-seq and m6A-seq techniques, we identified IRF7, a key transcription factor upstream of IFNs and ISGs, as one of the m6A modified targets during RV infection, and is essential to mediate the elevated anti-rotavirus immune response by METTL3 deficiency. These results identify *Irf7* as an important m6A target, and characterize, for the first time, the regulation of IFN response during RV infection in intestine, enabling a better understanding of how m6A modifications on mRNA regulate antiviral innate immune responses.

In addition to directly regulating target genes that involved in innate immune pathways, m6A modification is also known to affect viral gene expression, replication, and generation of progeny virions (***Roundtree et al., 2017***; ***Brocard et al., 2017***). Some viral RNA genomes are modified by m6A, such as simian virus 40 (***Tsai et al., 2018***; ***Lavi and Shatkin, 1975***), influenza A virus (***Krug et al., 1976***), adenovirus (***Sommer et al., 1976***), avian sarcoma virus (***Dimock and Stoltzfus, 1977***), Rous Sarcoma virus (***Kane and Beemon, 1985***), hepatitis C virus (***Gokhale et al., 2016***) and Zika virus (***Lichinchi et al., 2016***). Through our m6A-RIP-qPCR, Rotavirus RNA was also found to have m6A modification (***Figure 4—figure supplement 3***). Of note, genetic deletion of METTL3 in monkey kidney MA104 cell line, which has limited IFN responses (***Sánchez-Tacuba et al., 2020***), also led to reduced RV replication (***Figure 2—figure supplement 3***). Further, IRF7 deficiency didn't fully restore the suppressed rotaviral infection in *Mettl3*ΔIEC mice (***Figure 3e***). These results suggest that besides the contribution of *Irf7* to the resistant phenotype of rotavirus infection in IECs from *Mettl3*ΔIEC mice, other pathways (e.g. m6A modifications in RV RNA) may also play roles. The detailed mechanisms warrant further investigations in the future.

Intriguingly, m6A modifications were shown to maintain the genomic stability of mice embryonic stem cells by promoting the degradation of endogenous retrovirus (ERV) mRNA, or by regulating ERV heterochromatin and inhibiting its transcription (***Xu et al., 2021***; ***Chelmicki et al., 2021***). The absence of m6A results in the formation of abnormal endogenous dsRNA, which causes an aberrant immune response and necrosis in the hematopoietic system (***Gao et al., 2020***). In the intestine, through immunostaining with J2 antibody, we detected the increase of dsRNA levels in IECs of *Mettl3*ΔIEC mice compare to the littermate WT mice (***Figure 4—figure supplement 4***). In consistency, the aforementioned RNA-seq data showed that the expression of a set of ISGs including *Irf7* was significantly upregulated in *Mettl3* KO IECs. Our data suggest a dual activation model in steady state that in the absence of METTL3, the increase of dsRNA will induce the IFN responses, and the increased stability of *Irf7* mRNA, which serves as a key transcription factor of IFN and ISG expression, will amplify this process. Furthermore, m6A modification of viral RNA genomes affect the activation of innate sensor-mediated signaling (***Chen et al., 2021***; ***Kim et al., 2020***). Decreased m6A modification on RV genomes may activate innate sensors directly and induce higher IFN response, which will also be amplified by increase of *Irf7* mRNA stability.

Although m6A is involved in many important biological processes, the regulation of m6A modifications remain poorly understood. Here, we found RV infection down-regulates the level of m6A eraser ALKBH5 to induce m6A modifications, in an NSP1 dependent manner. The precise mechanism remains to be examined. As a result, ALKBH5 deficiency in IECs results in normal susceptibility to RV infection. In addition, the global m6A modification on mRNA transcripts declines by ages in the intestine, with a significant drop from 2 to 3 weeks post birth, which implicate the drop of RV infectivity in

adult mice vs neonatal mice. The dual regulation of m6A levels during RV infection and development provide new insights into the choice of either RV or the host on regulation of m6A modification to achieve either immune evasion or immune surveillance, respectively.

In conclusion, our work shed light into a novel role of m6A modifications in RV infection in vivo, and reported a tissue specific regulation of m6A during RV infection or development (***Figure 4g***). Future studies on tissue-specific regulation of m6A modification by viral infections in other tissues and organs (e.g. lung, liver) will be of interest.

Materials and methods

Mice

METTL3 conditional knockout mice were generated by inserting two loxp sites into the intron after the first exon and the intron before the last exon of *Mettl3* using CRISPR/cas9-based genome-editing system as previously described (***Li et al., 2017***). ALKBH5 conditional knockout mice were generated by inserting two loxp sites into the introns flanking the first exon of *Alkbh5* using CRISPR/cas9-based genome-editing system as previously described (***Zhou, 2021***). Genotyping of *Mettl3*$^{fl/fl}$ mice, *Alkbh5*$^{fl/fl}$ mice, *Vil1*^{Cre} mice (The Jackson Laboratory, Stock No: 021504), and *Irf7*$^{-/-}$ mice (RIKEN BRC, RBRC01420) were confirmed by PCR using primers as list below:

Mettl3$^{fl/fl}$ mice

Mettl3-L1+: CCCAACAGAGAAACGGTGAG
Mettl3-L2-: GGGTTCAACTGTCCAGCATC

Vil1^{Cre} mice

Vil1^{Cre}-182/150 F: GCCTTCTCCTCTAGGCTCGT
Vil1^{Cre}-182-R: TATAGGGCAGAGCTGGAGGA
Vil1^{Cre}-150-R: AGGCAAATTTTGGTGTACGG

Irf7$^{-/-}$ mice

RBRC01420-*Irf7*-WT-F: GTGGTACCCAGTCCTGCCCTCTTTATAATCT
RBRC01420-*Irf7*-Mut-F: TCGTGCTTTACGGTATCGCCGCTCCCGATTC
RBRC01420-*Irf7*-R: AGTAGATCCAAGCTCCCGGCTAAGTTCGTAC

Alkbh5$^{fl/fl}$ mice

Alkbh5-L1+: GCACAGTGGAGCACATCATG
Alkbh5-L2-: CAGAGGGCAAGCAACCACAC

The sex-, age-, and background-matched littermates of the knockout or conditional knockout mice were used as the controls in the present study. All mice were on the C57BL/6 background. Mice were maintained in SPF conditions under a strict 12 hr light cycle (lights on at 08:00 and off at 20:00). All animal studies were performed according to approved protocols by the Ethics Committee at the University of Science and Technology of China (USTCACUC202101016).

Cell culture

The MA104 cell line was obtained from the Cell Resource Center, Peking Union Medical College (which is the headquarter of National Infrastructure of Cell Line Resource). HEK293T (ATCC CRL-3216), HT-29 (ATCC HTB-38D) were obtained from the American Type Culture Collection (ATCC). MODE-K cell were obtained from Shanghai HonSun Biological Technology Co., Ltd.

The identity of these cell lines were authenticated with STR profiling (FBI, CODIS). All these cells were cultured in Dulbecco's modified Eagle's medium (DMEM) (Hyclone) supplemented with 10% fetal bovine serum (FBS) (Clark); All cells were cultured at 37 °C in 5% CO_2. All cells were tested for eliminating the possibility of mycoplasma contamination.

Poly(I:C) transfection

Poly(I:C) (OKA, A55994) was transfected at a concentration of 2 μg/ml using Lipofectamine 3,000 (Invitrogen) according to the manufacturer's protocol. Cells were analyzed at indicated hours.

Plasmids and SgRNAs

pSIN-m*Alkbh5*-3xflag and pLVX-m*Alkbh5*-puro was constructed by cloning mouse *Alkbh5* CDS into pSIN-3xflag and pLVX-puro plasmid.
pLVX-m*Irf7*-wt-puro was constructed by cloning mouse *Irf7* CDS and 3'UTR into pLVX-puro.
pLVX-m*Irf7*-Mut-puro was constructed by cloning mutated mouse *Irf7* CDS and 3'UTR into pLVX-puro. (The potential m6A modification sites (1400 A, 2213 A, 2693 A, 2927 A, 3446 A, 3475 A, 3491 A, 3590 A and 3620 A of mice *Irf7*(NC_000073)) were predicted on SRAMP website. The A to G mutation in these sites did not change the amino acids).

All gene silencing was done using a CRISPR–cas9 system, with lentiCRISPR v2 plasmid (Addgene no. 52961). The following sgRNAs were cloned downstream of the U6 promoter:

Human, rhesus and mouse *METTL3*/*Mettl3*: GGACACGTGGAGCTCTATCC;
Mouse *Alkbh5*: CCTCGTAGTCGCTGCGCTCG;
Mouse *Fto*: GAAGCGCGTCCAGACCGCGG;

Lentiviruses were generated by co-transfection of lentiCRISPR v2 constructs and packaging plasmids (psPAX2, Addgene no. 12,260 and pMD2.G, Addgene no. 12259), using PEI DNA transfection reagent (Shanghai maokang biotechnology), into HEK293T cells, according to the manufacturer's instructions. At 48 hr post transfection, supernatants were collected and filtered through a 0.22 μm polyvinylidene fluoride filter (Millex). To induce gene silencing, cells were transduced with lentivirus expressing sgRNA and were puromycin selected (2 μg/ml) for 4–5 days. The depletion of target proteins was confirmed by immunoblot analysis.

Virus infections

Rhesus and simian RV strains, including RRV (Rhesus), SA11-4F (simian), SA11-NSP1null (simian) were propagated in MA104 cells as previously described (***Ding et al., 2016***). Viruses were activated by trypsin (5 μg/ml) at 37 °C for 30 min prior to infection. Cells were washed with PBS three times and incubated with RV at different MOIs at 37 °C for 1 hr. After removal of RV inoculum, cells were washed with PBS, cultured in serum-free medium (SFM) and harvested for qPCR and western blot analysis at indicated time points.

EW stock virus was prepared by infecting 5-day-old C57BL/6 J mice, and harvesting crude centrifugation-clarified intestinal homogenate as previously described (***Ding et al., 2018***).

For all rotavirus infection except indicated elsewhere, 8-day-old wild-type mice, or genetically deficient mice were orally inoculated by gavage with RV EW virus as previously described (***Ding et al., 2018***). Mice were sacrificed, stool and small intestinal tissue were collected at indicated time points post infection. Viral loads in intestinal tissues and feces were detected by RT–qPCR.

Quantitative analysis of m6A level

The m6A analysis by LC-MS/MS was performed by Metware Biotechnology Co., Ltd (Wuhan, China). In brief, 1 μg purified RNA was digested into single nucleosides with 1 U nuclease P1 (Takara) and 1 U rSAP (Takara) and incubated at 37 °C. The digested RNA was injected into a LC-MS/MS which includes the ultra-performance liquid chromatography with a C18 column. The positive ion multiple reaction-monitoring (MRM) mode was adopted to detect m6A abundance. m6A levels were calculated from the standard curve which was generated from pure nucleoside standards.

RT-qPCR

For cells and tissues, total RNA was extracted with TRNzol Universal reagent (Tiangen) in accordance with the manufacturer's instructions. Real-time PCR was performed using SYBR Premix Ex Taq II (Tli RNaseH Plus) (Takara) and complementary DNA was synthesized with a PrimeScript RT reagent Kit with gDNA Eraser (Takara). The target genes were normalized to the housekeeping gene (*Gapdh*, *HPRT*) shown as $2^{-\Delta Ct}$. The used primers are as follows:

Primers detect mouse genes

Mettl3-F: ATTGAGAGACTGTCCCCTGG
Mettl3-R: AGCTTTGTAAGGAAGTGCGT
Mettl14-F: AGACGCCTTCATCTCTTTGG
Mettl14-R: AGCCTCTCGATTT CCTCTGT
Fto-F: CTGAGGAAGGAGTGGCATG
Fto-R: TCTCCACCTAAGACTTGTGC
Alkbh5-F: ACAAGATTAGATGCACCGCG
Alkbh5-R: TGTCCATTTCCAGGATCCGG
Wtap-F: GTTATGGCACGGGATGAGTT
Wtap-R: ATCTCCTGCTCTTTGGTTGC
Gapdh-F: TGAGGCCGGTGCTGAGTATGTCG
Gapdh-R: CCACAGTCTTCTGGGTGGCAGTG
Hprt-F: ACCTCTCGAAGTGTTGGATACAGG
Hprt-R: CTTGCGCTCATCTTAGGCTTTG
Irf7-F: ATGCACAGATCTTCAAGGCCTGGGC
Irf7-R: GTGCTGTGGAGTGCACAGCGGAAGT
Isg15-F: GGTGTCCGTGACTAACTCCAT
Isg15-R: TGGAAAGGGTAAGACCGTCCT
Oas1a-F: GCCTGATCCCAGAATCTATGC
Oas1a-R: GAGCAACTCTAGGGCGTACTG
Ifnb-F: TCCGAGCAGAGATCTTCAGGAA
Ifnb-R: TGCAACCACCACTCATTCTGAG
Ifnl3-F: AGCTGCAGGCCTTCAAAAAG
Ifnl3-R: TGGGAGTGAATGTGGCTCAG
Ifit1-F: GAACCCATTGGGGATGCACAACCT
Ifit1-R: CTTGTCCAGGTAGATCTGGGCTTCT

Primers detect human genes

GAPDH-F: ATGACATCAAGAAGGTGGTG
GAPDH-R: CATACCAGGAAATGAGCTTG
IRF7-F: CGAGACGAAACTTCCCGTCC
IRF7-R: GCTGATCTCTCCAAGGAGCC
IFNL3-F: TAAGAGGGCCAAAGATGCCTT
IFNL3-R: CTGGTCCAAGACATCCCCC
CXCL10-F: TGGCATTCAAGGAGTACCTC
CXCL10-R: TTGTAGCAATGATCTCAACACG
IFIT1-F: CAACCATGAGTACAAATGGTG
IFIT1-R: CTCACATTTGCTTGGTTGTC

Primers detect rhesus genes

Rhesus-*GAPDH*-F: ATGACATCAAGAAGGTGGTG
Rhesus-*GAPDH*-R: CATACCAGGAAATGAGCTTG
Rhesus-*IFIT1*-F: CAACCATGAGTACAAATGGTG
Rhesus-*IFIT1*-R: CTCACACTTGCTTGGTTGTC
Rhesus-*IRF7*-F: GTTCGGAGAGTGGCTCCTTG
Rhesus-*IRF7*-R: TCACCTCCTCTGCTGCTAGG
Rhesus-*IFNL1*-F: ACTCATACGGGACCTGACAT
Rhesus-*IFNL1*-R: GGATTCGGGGTGGGTTGAC
Rhesus-*IFNb*-F: GAGGAAATTAAGCAGCCGCAG
Rhesus-*IFNb*-R: ATTAGCAAGGAAGTTCTCCACA

Primers detect virus genes

Rotavirus EW-NSP2-F: GAGAATGTTCAAGACGTACTCCA
Rotavirus EW-NSP2-R: CTGTCATGGTGGTTTCAATTTC
Rotavirus EW-VP4-F: TGGCAAAGTCAATGGCAACG

Rotavirus EW-VP4-R: CCGAGACACTGAGGAAGCTG
Rotavirus EW-VP7-F: TCAACCGGAGACATTTCTGA
Rotavirus EW-VP7-R: TTGCGATAACGTGTCTTTCC
RRV VP7-F: ACGGCAACATTTGAAGAAGTC
RRV VP7-R: TGCAAGTAGCAGTTGTAACATC
RRV NSP2-F: GAGAATCATCAGGACGTGCTT
RRV NSP2-R: CGGTGGCAGTTGTTTCAAT
RRV NSP5-F: CTGCTTCAAACGACCCACTCAC
RRV NSP5-R: TGAATCCATAGACACGCC

m6A Dot blot assay

Total RNA was isolated from mice ileum using TRNzol Universal Reagent (Tiangen, Lot#U8825) according to the manufacturer's instructions. RNA samples were quantified using UV spectrophotometry and denatured at 95 °C for 3 min. The m6A-dot-blot was performed according to a published work (***Shen et al., 2016***). In brief, the primary rabbit anti-m6A antibody (1:5000, Synaptic System, #202003) or the primary rabbit anti-m6A antibody (1:1000, Sigma-Aldrich, ABE572-I-100UG) was applied to the Amersham Hybond-N+ membrane (GE Healthcare, USA) containing RNA samples. Dot blots were visualized by the imaging system after incubation with secondary antibody HRP-conjugated Goat anti-rabbit IgG (Beyotime, A0208).

Western blot

Briefly, cells and tissue were lysed with RIPA buffer (Beyotime Biotechnology) supplemented with PMSF (Beyotime Biotechnology) and protease inhibitor cocktail (Roche). METTL3 (abcam, ab195352, 1:2000), METTL14 (sigma, HPA038002, 1:2000), ALKBH5 (sigma, HPA007196, 1:2000), FTO (abcam, ab92821), NSP1 and VP6 (gift from Harry B. Greenberg lab), GAPDH (proteintech), TUBULIN (proteintech), beta-ACTIN (proteintech), Phospho-IRF-7 (Ser437/438) (D6M2I) (CST), Phospho-TBK1/NAK (Ser172) (D52C2) (CST), TBK1/NAK (D1B4) (CST), and IRF-7 (D8V1J) (CST) antibodies were used in accordance with the manufacturer's instructions. After incubation with the primary antibody overnight, the blotted PVDF membranes (Immobilon, IPVH00010) were incubated with goat anti-rabbit IgG-HRP (Beyotime, A0208) or goat anti-mouse IgG-HRP (Beyotime, A0216) and exposed with BIO-RAD ChemiDocTM Imaging System for a proper exposure period.

RNA degradation assay

The stability of targeted mRNA was assessed as previously described (***Li et al., 2017***). In brief, METTL3 knock down HT-29 and control cell were plated on 24-well plate. Actinomycin-D (MCE, HY17559) was added to a final concentration of 5 μM, and cells were harvested by indicated time points after actinomycin-D treatment. The RNA samples are processed and qPCR was used to measure the mRNA transcripts, all data were normalized to that of t = 0 time point.

Dual-luciferase assay

pmirGLO (Firefly luciferase, hRluc) vector of the Dual-luciferase Reporter assay system (Promega, E1910) was used to determine the function of m6A modification within the 3'UTR of *Irf7* transcripts. The potential m6A modification sites (3446 A, 3475 A, 3491 A, 3590 A, and 3620 A of mice *Irf7*(NC_000073)) were predicted on SRAMP website. The mutants harbor the A to G mutations at these sites. The assay was performed according to the manufacture's instruction of Promega Dual-Luciferase Reporter Assay System(E1910): Briefly, 300 ng of pmirGLO vector containing *Irf7*-3'UTR or m6A-mutant *Irf7*-3'UTR were transfected into HEK293T cells in triplicate wells. The relative luciferase activity was accessed 36 hr post-transfection.

Isolation of IECs in the Intestine

Small intestines were excised and flushed thoroughly three times with PBS. They were turned inside out and cut into ~1 cm sections then transferred into RPMI with 2 mM EDTA, and shaken for 15 min at 37 °C. Supernatants were collected through a 100-mm cell strainer to get single-cell suspensions. Cells were collected as the IEC fraction which contains both epithelial cells (~90%) and lymphocytes (IEL, ~ 10%). Single-cell suspension was used for further analysis.

RNA-Seq

IECs from *Mettl3*ΔIEC mice as well as the wild-type littermate control mice were isolated as described in previous section. Total RNAs were extracted with TRNzol universal RNA Reagen kits. Berrygenomics (Beijing, China) processed the total RNA and constructed the mRNA libraries, and subject them to standard illumine sequencing on Novaseq 6,000 system, and obtained >40 million Pair-end 150 reads for each sample. Raw RNA-sequencing reads were aligned to the mouse genome (mm10, GRCm38) with STAR (v2.5.3a). Gene expression levels and differential analysis was performed with edgeR(v3.29.2). Genes were considered significantly differentially expressed if showing ≥1.5 fold change and FDR < 0.05. Gene set analysis was performed and enriched pathways were obtained through online bioinformatics tools (metascape) and GSEA (v4.0.3). Pathway plot were gene-rated with R package 'ggplot2' (***Li et al., 2017***).

m6A RNA-IP-qPCR and m6A RNA-IP-Seq

m6A RNA-IP-Seq was carried out according to a previously published protocol (***Li et al., 2017***). In brief, total cellular RNA extracted from WT C57 mice IEC was fragmented by ZnCl2 followed by ethanol precipitation. Fragmented RNA was incubated with an anti-m6A antibody (Sigma Aldrich ABE572-I) or IgG IP Grade Rabbit polyclonal antibody (abcam, lot: 934197). The eluted RNA and input were subjected to high-throughput sequencing using standard protocols (Illumina, San Diego, CA, USA) or processed as described in 'RT-qPCR' section, except that the data were normalized to the input samples. The m6A RIP-Seq data were analyzed as described previously (***Li et al., 2017***).

RIP-*Ptpn4*-F: CCTCCCATCCCGGTCTCCACC
RIP-*Ptpn4*-R: GGCTGCCCATCTTCAGGGGT
RIP-*Rps14*-F: ACCTGGAGCCCAGTCAGCCC
RIP-*Rps14*-R: CACAGACGGCGACCACGACG
RIP-*Tlr3*-F: TGCTCAGGAGGGTGGCCCTT
RIP-*Tlr3*-R: CGGGGTTTGCGCGTTTCCAG
m6A-*Irf7*-F1: GACAGCAGCAGTCTCGGCTT
m6A-*Irf7*-R1: ACCCAGGTCCATGAGGAAGT
m6A-*Irf7*-F2: GGCAAGACTTGTCAGCAGGG
m6A-*Irf7*-R2: TAGACAAGCACAAGCCGAGAC

m6A sites on RV-EW RNA were predicted on http: //www.cuilab.cn/sramp website, and m6A-RIP-qPCR primer were designed on NCBI primer blast according to the predicted m6A sites.

m6A-RIP-qPCR primer

RIP-EW-VP1-F: ACGAAATGCTTGTTGCTATGAGT
RIP-EW-VP1-R: AACCTGTCCGTCAACCATTC
RIP-EW-VP2-F: GGCCAGAACAGGCTAAACAAC
RIP-EW-VP2-R: CGCAGTTCTCTTTCGCCATTT
RIP-EW-VP3-F: CGATGACAGCACAAAAGTCGG
RIP-EW-VP3-R: CGTGTCTCTTGCGAAGTC
RIP-EW-VP4-F: TCAGCAGACGGTTGAGACTG
RIP-EW-VP4-R: GGCTGAGATGTCATCGAAGTT
RIP-EW-NSP1-F: CCTCACATCTCTGCTACATGAACT
RIP-EW-NSP1-R: TGCTGGTTGGACATGGAATGA
RIP-EW-VP6-F: CTGCACTTTTCCCAAATGCTCA
RIP-EW-VP6-R: GAGTCAATTCTAAGTGTCAGTCCG
RIP-EW-NSP3-F: CTTGACGTGGAGCAGCAAC
RIP-EW-NSP3-R: AATGTTTCAATGTCGTCCAACG
RIP-EW-NSP2-F: TCCACCACTCTAAAGAACTACTGC
RIP-EW-NSP2-R: TCCGCTGTCATGGTGGTTTC
RIP-EW-VP7-F: TCGGAACTTGCAGACTTGAT
RIP-EW-VP7-R: GCTTCGTCTGTTTGCTGGTA
RIP-EW-NSP4-F: TGCACTGACTGTTCTATTTACGA
RIP-EW-NSP4-R: GGGAAGTTCGCATTGCTAGT
RIP-EW-NSP5/6-F: GGACACCGCAAGGTCAAAAA
RIP-EW-NSP5/6-R: TCGTCTGAGTCTGATTCTGCTT

J2 immunofluorescent staining

IECs from *Mettl3*ΔIEC mice as well as from the wild-type littermate control mice were isolated as described in previous section. Isolated IEC were centrifuged onto glass slides and fixed with 4% Paraformaldehyde for 30 min at room temperature. Subsequently, permeabilized and blocked with PBS containing 0.1% Triton-X-100% and 5% bovine serum albumin for 1 hr at room temperature. Double-stranded RNA (dsRNA) was labeled by a mouse monoclonal antibody J2 (Scisons) for 2 hr at room temperature, followed by incubation with anti-mouse IgG Alexa Fluor 594-conjugated antibody (Invitrogen) for 1 hr, and cells nuclei were visualized with 4,6-diamidino-2-phenylindole (DAPI, Invitrogen). All fluorescence images were analyzed via confocal imaging using Zeiss LSM880.

Statistical analysis

Statistical analysis was performed with the GraphPad Prism 8.0 (GraphPad, Inc, USA). Experiments were independently repeated for indicated times listed in the figure legend. Representative data was exhibited as the means ± SEM. Quantitative data was compared using Student's t test. In addition, correlational analysis of gene expression was conducted with linear regression. p-values for every result were labeled on figures, and $p < 0.05$ was reckoned as statistically significant (*$p < 0.05$, **$p < 0.01$, ***$p < 0.001$, ****$p < 0.0001$, NS., not significant).

Acknowledgements

We would like to thank Hongdi Ma, Taidou Hu, Kaixin He, Yinglei Wang, Ji Hu, Anlei Wang, and Meng Guo for technical help and helpful discussion. This work was supported by grants from the Strategic Priority Research Program of the Chinese Academy of Sciences (XDB29030101)(SZ), the National Key R&D Program of China (2018YFA0508000)(SZ), and National Natural Science Foundation of China (81822021, 91842105, 31770990, 82061148013, 81821001)(SZ).

Additional information

Funding

Funder	Grant reference number	Author
Chinese Academy of Sciences	Strategic Priority Research Program (XDB29030101)	Shu Zhu
National Key Research and Development Program of China	2018YFA0508000	Shu Zhu
National Natural Science Foundation of China	81822021	Shu Zhu
National Natural Science Foundation of China	91842105	Shu Zhu
National Natural Science Foundation of China	31770990	Shu Zhu
National Natural Science Foundation of China	82061148013	Shu Zhu
National Natural Science Foundation of China	81821001	Shu Zhu

The funders had no role in study design, data collection and interpretation, or the decision to submit the work for publication.

Author contributions

Anmin Wang, Data curation, Writing - original draft; Wanyiin Tao, Data curation; Jiyu Tong, Juanzi Gao, Jinghao Wang, Gaopeng Hou, Chen Qian, Guorong Zhang, Runzhi Li, Decai Wang, Xingxing Ren, Kaiguang Zhang, Wen Pan, Investigation; Siyuan Ding, Writing – review and editing; Richard

A Flavell, Resources; Huabing Li, Conceptualization, Resources; Shu Zhu, Conceptualization, Project administration, Resources, Writing – review and editing

Author ORCIDs
Anmin Wang http://orcid.org/0000-0003-2239-9051
Richard A Flavell http://orcid.org/0000-0003-4461-0778
Shu Zhu http://orcid.org/0000-0002-8163-0869

Ethics
All animal studies were performed according to approved protocols by the Ethics Committee at the University of Science and Technology of China (USTCACUC202101016).

Decision letter and Author response
Decision letter https://doi.org/10.7554/eLife.73628.sa1
Author response https://doi.org/10.7554/eLife.73628.sa2

Additional files

Supplementary files
- Transparent reporting form
- Source data 1. Source data for ***Figures 1–4***, ***Figure 1—figure supplements 1–4***, ***Figure 2—figure supplements 1–5***, ***Figure 4—figure supplements 1–4***.

Data availability
RNA sequencing data are available from the SRA database with accession numbers PRJNA713535. All data generated or analysed during this study are included in the manuscript and supporting file; source data files are in Dryad. Source data contain the numerical data used to generate the figures.

The following datasets were generated:

Author(s)	Year	Dataset title	Dataset URL	Database and Identifier
Wang A	2022	Data from: m6A modifications regulate intestinal immunity and rotavirus infection	http://dx.doi.org/10.5061/dryad.p2ngf1vr8	Dryad Digital Repository, 10.5061/dryad.p2ngf1vr8
Wang A	2022	m6A modifications regulate intestinal immunity and rotavirus infection	https://www.ncbi.nlm.nih.gov/sra/query/acc.cgi?accPRJNA713535	NCBI Sequence Read Archive, PRJNA713535

References

Barro M, Patton JT. 2005. Rotavirus nonstructural protein 1 subverts innate immune response by inducing degradation of IFN regulatory factor 3. *PNAS* **102**:4114–4119. DOI: https://doi.org/10.1073/pnas.0408376102, PMID: 15741273

Barro M, Patton JT. 2007. Rotavirus NSP1 inhibits expression of type I interferon by antagonizing the function of interferon regulatory factors IRF3, IRF5, and IRF7. *Journal of Virology* **81**:4473–4481. DOI: https://doi.org/10.1128/JVI.02498-06, PMID: 17301153

Brocard M, Ruggieri A, Locker N. 2017. m6A RNA methylation, a new hallmark in virus-host interactions. *Journal of General Virology* **98**:2207–2214. DOI: https://doi.org/10.1099/jgv.0.000910, PMID: 28869001

Chelmicki T, Roger E, Teissandier A, Dura M, Bonneville L, Rucli S, Dossin F, Fouassier C, Lameiras S, Bourc'his D. 2021. m6A RNA methylation regulates the fate of endogenous retroviruses. *Nature* **591**:312–316. DOI: https://doi.org/10.1038/s41586-020-03135-1, PMID: 33442060

Chen S, Kumar S, Espada CE, Tirumuru N, Cahill MP, Hu L, He C, Wu L. 2021. N6-methyladenosine modification of HIV-1 RNA suppresses type-I interferon induction in differentiated monocytic cells and primary macrophages. *PLOS Pathogens* **17**:e1009421. DOI: https://doi.org/10.1371/journal.ppat.1009421, PMID: 33690734

Ciancanelli MJ, Abel L, Zhang S-Y, Casanova J-L. 2016. Host genetics of severe influenza: from mouse Mx1 to human IRF7. *Current Opinion in Immunology* **38**:109–120. DOI: https://doi.org/10.1016/j.coi.2015.12.002, PMID: 26761402

Crawford SE, Ramani S, Tate JE, Parashar UD, Svensson L, Hagbom M, Franco MA, Greenberg HB, O'Ryan M, Kang G, Desselberger U, Estes MK. 2017. Rotavirus infection. *Nature Reviews. Disease Primers* **3**:17083. DOI: https://doi.org/10.1038/nrdp.2017.83, PMID: 29119972

Dimock K, Stoltzfus CM. 1977. Sequence specificity of internal methylation in B77 avian sarcoma virus RNA subunits. *Biochemistry* **16**:471–478. DOI: https://doi.org/10.1021/bi00622a021, PMID: 189800

Ding S, Mooney N, Li B, Kelly MR, Feng N, Loktev AV, Sen A, Patton JT, Jackson PK, Greenberg HB, Coyne CB. 2016. Comparative Proteomics Reveals Strain-Specific β-TrCP Degradation via Rotavirus NSP1 Hijacking a Host Cullin-3-Rbx1 Complex. *PLOS Pathogens* **12**:e1005929. DOI: https://doi.org/10.1371/journal.ppat.1005929, PMID: 27706223

Ding S, Zhu S, Ren L, Feng N, Song Y, Ge X, Li B, Flavell RA, Greenberg HB. 2018. Rotavirus VP3 targets MAVS for degradation to inhibit type III interferon expression in intestinal epithelial cells. *eLife* **7**:e39494. DOI: https://doi.org/10.7554/eLife.39494, PMID: 30460894

Dominissini D, Moshitch-Moshkovitz S, Schwartz S, Salmon-Divon M, Ungar L, Osenberg S, Cesarkas K, Jacob-Hirsch J, Amariglio N, Kupiec M, Sorek R, Rechavi G. 2012. Topology of the human and mouse m6A RNA methylomes revealed by m6A-seq. *Nature* **485**:201–206. DOI: https://doi.org/10.1038/nature11112, PMID: 22575960

Du J, Lan Z, Liu Y, Liu Y, Li Y, Li X, Guo T. 2017. Detailed analysis of BALB/c mice challenged with wild type rotavirus EDIM provide an alternative for infection model of rotavirus. *Virus Research* **228**:134–140. DOI: https://doi.org/10.1016/j.virusres.2016.12.001, PMID: 27932206

Gao Y, Vasic R, Song Y, Teng R, Liu C, Gbyli R, Biancon G, Nelakanti R, Lobben K, Kudo E, Liu W, Ardasheva A, Fu X, Wang X, Joshi P, Lee V, Dura B, Viero G, Iwasaki A, Fan R, et al. 2020. m6A Modification Prevents Formation of Endogenous Double-Stranded RNAs and Deleterious Innate Immune Responses during Hematopoietic Development. *Immunity* **52**:1007–1021. DOI: https://doi.org/10.1016/j.immuni.2020.05.003, PMID: 32497523

Gokhale NS, McIntyre ABR, McFadden MJ, Roder AE, Kennedy EM, Gandara JA, Hopcraft SE, Quicke KM, Vazquez C, Willer J, Ilkayeva OR, Law BA, Holley CL, Garcia-Blanco MA, Evans MJ, Suthar MS, Bradrick SS, Mason CE, Horner SM. 2016. N6-Methyladenosine in Flaviviridae Viral RNA Genomes Regulates Infection. *Cell Host & Microbe* **20**:654–665. DOI: https://doi.org/10.1016/j.chom.2016.09.015, PMID: 27773535

Hao H, Hao S, Chen H, Chen Z, Zhang Y, Wang J, Wang H, Zhang B, Qiu J, Deng F, Guan W. 2019. N6-methyladenosine modification and METTL3 modulate enterovirus 71 replication. *Nucleic Acids Research* **47**:362–374. DOI: https://doi.org/10.1093/nar/gky1007, PMID: 30364964

Hesser CR, Karijolich J, Dominissini D, He C, Glaunsinger BA. 2018. N6-methyladenosine modification and the YTHDF2 reader protein play cell type specific roles in lytic viral gene expression during Kaposi's sarcoma-associated herpesvirus infection. *PLOS Pathogens* **14**:e1006995. DOI: https://doi.org/10.1371/journal.ppat.1006995, PMID: 29659627

Honda K, Yanai H, Negishi H, Asagiri M, Sato M, Mizutani T, Shimada N, Ohba Y, Takaoka A, Yoshida N, Taniguchi T. 2005. IRF-7 is the master regulator of type-I interferon-dependent immune responses. *Nature* **434**:772–777. DOI: https://doi.org/10.1038/nature03464, PMID: 15800576

Imam H, Khan M, Gokhale NS, McIntyre ABR, Kim GW, Jang JY, Kim SJ, Mason CE, Horner SM, Siddiqui A. 2018. N6-methyladenosine modification of hepatitis B virus RNA differentially regulates the viral life cycle. *PNAS* **115**:8829–8834. DOI: https://doi.org/10.1073/pnas.1808319115, PMID: 30104368

Kanai Y, Komoto S, Kawagishi T, Nouda R, Nagasawa N, Onishi M, Matsuura Y, Taniguchi K, Kobayashi T. 2017. Entirely plasmid-based reverse genetics system for rotaviruses. *PNAS* **114**:2349–2354. DOI: https://doi.org/10.1073/pnas.1618424114, PMID: 28137864

Kane SE, Beemon K. 1985. Precise localization of m6A in Rous sarcoma virus RNA reveals clustering of methylation sites: implications for RNA processing. *Molecular and Cellular Biology* **5**:2298–2306. DOI: https://doi.org/10.1128/mcb.5.9.2298-2306.1985, PMID: 3016525

Kim GW, Imam H, Khan M, Siddiqui A. 2020. N 6-Methyladenosine modification of hepatitis B and C viral RNAs attenuates host innate immunity via RIG-I signaling. *The Journal of Biological Chemistry* **295**:13123–13133. DOI: https://doi.org/10.1074/jbc.RA120.014260, PMID: 32719095

Krug RM, Morgan MA, Shatkin AJ. 1976. Influenza viral mRNA contains internal N6-methyladenosine and 5'-terminal 7-methylguanosine in cap structures. *Journal of Virology* **20**:45–53. DOI: https://doi.org/10.1128/jvi.20.1.45-53.1976

Lavi S, Shatkin AJ. 1975. Methylated simian virus 40-specific RNA from nuclei and cytoplasm of infected BSC-1 cells. *PNAS* **72**:2012–2016. DOI: https://doi.org/10.1073/pnas.72.6.2012, PMID: 166375

Li HB, Tong J, Zhu S, Batista PJ, Duffy EE, Zhao J, Bailis W, Cao G, Kroehling L, Chen Y, Wang G, Broughton JP, Chen YG, Kluger Y, Simon MD, Chang HY, Yin Z, Flavell RA. 2017. m6A mRNA methylation controls T cell homeostasis by targeting the IL-7/STAT5/SOCS pathways. *Nature* **548**:338–342. DOI: https://doi.org/10.1038/nature23450, PMID: 28792938

Lichinchi G, Zhao BS, Wu Y, Lu Z, Qin Y, He C, Rana TM. 2016. Dynamics of Human and Viral RNA Methylation during Zika Virus Infection. *Cell Host & Microbe* **20**:666–673. DOI: https://doi.org/10.1016/j.chom.2016.10.002, PMID: 27773536

Lin J-D, Feng N, Sen A, Balan M, Tseng H-C, McElrath C, Smirnov SV, Peng J, Yasukawa LL, Durbin RK, Durbin JE, Greenberg HB, Kotenko SV. 2016. Distinct Roles of Type I and Type III Interferons in Intestinal Immunity to Homologous and Heterologous Rotavirus Infections. *PLOS Pathogens* **12**:e1005600. DOI: https://doi.org/10.1371/journal.ppat.1005600, PMID: 27128797

Liu Y. 2019. N (6)-methyladenosine RNA modification-mediated cellular metabolism rewiring inhibits viral replication. *Science (New York, N.Y.)* **365**:1171–1176. DOI: https://doi.org/10.1126/science.aax4468, PMID: 31439758

Pott J, Mahlakõiv T, Mordstein M, Duerr CU, Michiels T, Stockinger S, Staeheli P, Hornef MW. 2011. IFN-lambda determines the intestinal epithelial antiviral host defense. *PNAS* **108**:7944–7949. DOI: https://doi.org/10.1073/pnas.1100552108, PMID: 21518880

Roundtree IA, Evans ME, Pan T, He C. 2017. Dynamic RNA Modifications in Gene Expression Regulation. *Cell* **169**:1187–1200. DOI: https://doi.org/10.1016/j.cell.2017.05.045, PMID: 28622506

Rubio RM, Depledge DP, Bianco C, Thompson L, Mohr I. 2018. RNA m6 A modification enzymes shape innate responses to DNA by regulating interferon β. *Genes & Development* **32**:1472–1484. DOI: https://doi.org/10.1101/gad.319475.118, PMID: 30463905

Sánchez-Tacuba L, Feng N, Meade NJ, Mellits KH, Jaïs PH, Yasukawa LL, Resch TK, Jiang B, López S, Ding S, Greenberg HB. 2020. An Optimized Reverse Genetics System Suitable for Efficient Recovery of Simian, Human, and Murine-Like Rotaviruses. *Journal of Virology* **94**:18. DOI: https://doi.org/10.1128/JVI.01294-20, PMID: 32759316

Saxena K, Simon LM, Zeng XL, Blutt SE, Crawford SE, Sastri NP, Karandikar UC, Ajami NJ, Zachos NC, Kovbasnjuk O, Donowitz M, Conner ME, Shaw CA, Estes MK. 2017. A paradox of transcriptional and functional innate interferon responses of human intestinal enteroids to enteric virus infection. *PNAS* **114**:E570–E579. DOI: https://doi.org/10.1073/pnas.1615422114, PMID: 28069942

Shen L, Liang Z, Gu X, Chen Y, Teo ZWN, Hou X, Cai WM, Dedon PC, Liu L, Yu H. 2016. N(6)-Methyladenosine RNA Modification Regulates Shoot Stem Cell Fate in Arabidopsis. *Developmental Cell* **38**:186–200. DOI: https://doi.org/10.1016/j.devcel.2016.06.008, PMID: 27396363

Sommer S, Salditt-Georgieff M, Bachenheimer S, Darnell JE, Furuichi Y, Morgan M, Shatkin AJ. 1976. The methylation of adenovirus-specific nuclear and cytoplasmic RNA. *Nucleic Acids Research* **3**:749–765. DOI: https://doi.org/10.1093/nar/3.3.749, PMID: 1272797

Tsai K, Courtney DG, Cullen BR. 2018. Addition of m6A to SV40 late mRNAs enhances viral structural gene expression and replication. *PLOS Pathogens* **14**:e1006919. DOI: https://doi.org/10.1371/journal.ppat.1006919, PMID: 29447282

Winkler R, Gillis E, Lasman L, Safra M, Geula S, Soyris C, Nachshon A, Tai-Schmiedel J, Friedman N, Le-Trilling VTK, Trilling M, Mandelboim M, Hanna JH, Schwartz S, Stern-Ginossar N. 2019. m6A modification controls the innate immune response to infection by targeting type I interferons. *Nature Immunology* **20**:173–182. DOI: https://doi.org/10.1038/s41590-018-0275-z, PMID: 30559377

Xu W, Li J, He C, Wen J, Ma H, Rong B, Diao J, Wang L, Wang J, Wu F, Tan L, Shi YG, Shi Y, Shen H. 2021. METTL3 regulates heterochromatin in mouse embryonic stem cells. *Nature* **591**:317–321. DOI: https://doi.org/10.1038/s41586-021-03210-1, PMID: 33505026

Xuan J-J, Sun W-J, Lin P-H, Zhou K-R, Liu S, Zheng L-L, Qu L-H, Yang J-H. 2018. RMBase v2.0: deciphering the map of RNA modifications from epitranscriptome sequencing data. *Nucleic Acids Research* **46**:D327–D334. DOI: https://doi.org/10.1093/nar/gkx934, PMID: 29040692

Ye F, Chen ER, Nilsen TW. 2017. Kaposi's Sarcoma-Associated Herpesvirus Utilizes and Manipulates RNA N6-Adenosine Methylation To Promote Lytic Replication. *Journal of Virology* **91**:e00466-17. DOI: https://doi.org/10.1128/JVI.00466-17, PMID: 28592530

Zhou J. 2021. m(6)A demethylase ALKBH5 controls CD4(+) T cell pathogenicity and promotes autoimmunity. *Science Advances* **7**:25. DOI: https://doi.org/10.1126/sciadv.abg0470